Bioorganic & Medicinal Chemistry 19 (2011) 1666–1673

Contents lists available at ScienceDirect

Bioorganic & Medicinal Chemistry

journal homepage: www.elsevier.com/locate/bmc

Radiosynthesis and in vivo evaluation of [^{11}C]MP-10 as a PET probe for imaging PDE10A in rodent and non-human primate brain

Zhude Tu [a,*], Jinda Fan [a], Shihong Li [a], Lynne A. Jones [a], Jinquan Cui [a], Prashanth K. Padakanti [a], Jinbin Xu [a], Dexing Zeng [a], Kooresh I. Shoghi [a], Joel S. Perlmutter [a,b], Robert H. Mach [a]

[a] Department of Radiology, Washington University School of Medicine, Mallinckrodt Institute of Radiology, 510 South Kingshighway Blvd., St. Louis, MO 63110, USA
[b] Department of Neurology, Washington University School of Medicine, 510 South Kingshighway Blvd., St. Louis, MO 63110, USA

ARTICLE INFO

Article history:
Received 14 December 2010
Revised 13 January 2011
Accepted 16 January 2011
Available online 22 January 2011

Keywords:
PDE10A
PET imaging
Carbon-11
MP-10
Huntington's disease

ABSTRACT

2-((4-(1-[^{11}C]Methyl-4-(pyridin-4-yl)-1*H*-pyrazol-3-yl)phenoxy)methyl)-quinoline (MP-10), a specific PDE10A inhibitor (IC_{50} = 0.18 nM with 100-fold selectivity over other PDEs), was radiosynthesized by alkylation of the desmethyl precursor with [^{11}C]CH_3I, ~45% yield, >92% radiochemical purity, >370 GBq/μmol specific activity at end of bombardment (EOB). Evaluation in Sprague–Dawley rats revealed that [^{11}C]MP-10 had highest brain accumulation in the PDE10A enriched-striatum, the 30 min striatum: cerebellum ratio reached 6.55. MicroPET studies of [^{11}C]MP-10 in monkeys displayed selective uptake in striatum. However, a radiolabeled metabolite capable of penetrating the blood–brain-barrier may limit the clinical utility of [^{11}C]MP-10 as a PDE10A PET tracer.

1. Introduction

Phosphodiesterase 10A (PDE10A) is a unique dual specificity phosphodiesterase that converts both cyclic adenosine monophosphate (cAMP) to adenosine monophosphate (AMP) and cyclic guanosine monophosphate (cGMP) to guanosine monophosphate (GMP).[1,2] Unlike other phosphodiesterase (PDE) families, PDE10A is uniquely expressed in the brain where it plays a critical role in dopaminergic neurotransmission.[3,4] The expression of PDE10A is highest in the medium spiny neurons of the striatum (caudate and putamen), nucleus accumbens, and olfactory tubercle of mice, dogs, cynomolgus and humans.[5] Abnormal striatal levels of PDE10A impair striatal output that may contribute substantially to the pathophysiology of schizophrenia, Huntington's disease (HD), Parkinson disease (PD), Tourette syndrome, and drug abuse.[6–9] PDE10A plays a major role in the regulation of cyclic nucleotide signaling cascades; inhibition of the enzyme causes cAMP response element-binding (CREB) phosphorylation and activation.[10] For Huntington's disease, western analysis of 1 μg protein extracts from the striatum of R6/1 and R6/2 Huntington's disease mice prior to motor manifestation development displayed lower PDE10A proteins levels than in wild type mice, and may be an early marker of neuronal dysfunction. Post mortem analysis of human brain tissue has shown similar results: western analysis of 5 μg of total protein samples from the caudate, nucleus accumbens and putamen from three patients with grade 3 HD demonstrated reduced PDE10A protein levels compared with age-matched neurologically normal control subjects.[10–12] Inhibition studies with 2-{4-[pyridin-4-yl-1-(2,2,2-trifluoro-ethyl)-1*H*-pyrazol-3-yl]-phenoxymethyl}-quinoline (TP-10), an analogue of 2-((4-(1-methyl-4-(pyridin-4-yl)-1*H*-pyrazol-3-yl)phenoxy)-methyl)quinoline (MP-10, **7**) in a rodent quinolinic acid model of Huntington's disease suggest that PDE10A inhibition may be a novel neuroprotective approach to the treatment of HD. In addition to the potential application of PDE10A inhibitors in HD, the observation that PDE10A expression parallels D_2-receptor distribution suggests that PDE10A inhibition might yield therapeutic effects similar to D_2 antagonism for schizophrenia patients, without accompanying untoward effects. Inhibition of PDE10A in rodents significantly increased extra-cellular levels of cAMP in the striatum and also

Abbreviations: AMP, adenosine monophosphate; cAMP, cyclic adenosine monophosphate; CNS, central nervous system; cGMP, cyclic guanosine monophosphate; DMF, *N*,*N*-dimethylformamide; DMSO, dimethyl sulfoxide; GMP, guanosine monophosphate; HD, Huntington disease; LDA, lithium diisopropylamide; MP-10, 2-[4-(1-methyl-4-pyridin-4-yl-1*H*-pyrazol-3-yl)-phenoxymethyl]-quinoline; MSNs, medium-sized spiny neurons; PCP, phenylcyclohexylpiperidine; PDE10A, phosphodiesterase 10A; PDE3A, phosphodiesterase 3A; PDE3B, phosphodiesterase 3B; PET, positron emission tomography; THF, tetrahydrofuran; TLC, thin layer chromatography; TP-10, 2-{4-[-pyridin-4-yl-1-(2,2,2-trifluoro-ethyl)-1*H*-pyrazol-3-yl]-phenoxymethyl}-quinoline; MP-10, 2-[4-(1-methyl-4-pyridin-4-yl-1*H*-pyrazol-3-yl)-phenoxymethyl]-quinoline; EOB, end of bombardment.

* Corresponding author. Tel.: +1 314 362 8487; fax: +1 314 362 8555.
E-mail address: tuz@mir.wustl.edu (Z. Tu).

0968-0896/$ - see front matter © 2011 Elsevier Ltd. All rights reserved.
doi:10.1016/j.bmc.2011.01.032

mediated certain clinical antipsychotic effects[13,14] with significant differences from D_2-receptor antagonists in preclinical behavioral models of schizophrenia including the induction of catalepsy and prepulse inhibition of startle.[14,15]

Over the past 10 years, tremendous efforts have been made to develop PDE10A inhibitors for treatment of schizophrenia and associated mental disorders.[16–19] MP-10 has been identified as a promising therapeutic inhibitor of PDE10A and is in clinical evaluation.[16,17] However, most evidence supporting the role of PDE10A in CNS disorders comes from behavioral studies and post mortem tissue analysis. Positron emission tomography (PET) is a non-invasive imaging modality that can provide functional information about molecular and cellular processes in living subjects. Therefore, a PET radioligand having high affinity and selectivity for PDE10A would provide a unique tool to study changes in PDE10A levels of living subjects and investigate the physiological function of PDE10A in the CNS. Our group reported initial results for imaging PDE10A in vivo.[20,21] Recently, an initial validation of an MP-10 analogue, 2-((4-(1-[^{18}F]ethyl-4-(pyridin-4-yl)-1*H*-pyrazol-3-yl)phenoxy)-methyl)quinoline (^{18}F-JNJ41510417) was reported.[22] To confirm if MP-10 could serve as a PET probe for quantifying PDE10A in vivo, we radiosynthesized [^{11}C]MP-10 and conducted in vivo validation studies in rodent and non-human primate models. In this paper, we will describe the radiosynthesis of [^{11}C]MP-10, its biodistribution and validation in vivo in Sprague–Dawley rats, MicroPET imaging studies of [^{11}C]MP-10 in rhesus macaque, as well as the metabolite analysis of the rat brain tissue, plasma and monkey plasma post-injection of [^{11}C]MP-10 in animals.

2. Results and discussion

2.1. Chemistry

The target compound MP-10 is a pyrazole derivative, that possesses a methyl group on the nitrogen, which gives easy access to ^{11}C-labeling by N-methylation of the corresponding desmethyl precursor (**6**) with [^{11}C]methyl iodide ([^{11}C]CH_3I). The synthesis of the *N*-desmethyl precursor **6** and the standard compound **7** was accomplished by starting with methyl 4-hydroxybenzoate (**1**) as shown in Scheme 1 following the reported procedure.[16,23] However, reference compound **7** and its isomer **8** were synthesized from the key intermediate **5** by reacting it with methylhydrazine instead of following the literature procedure, in which 4-(1-methyl-4-pyridin-4-yl-1*H*-pyrazol-3-yl)-phenol was treated with quinoxaline-2-yl-methanol.[18] Compound 4-(1-methyl-4-pyridin-4-yl-1*H*-pyrazol-3-yl)-phenol that matched the major radiolabeled metabolite (**9**) was synthesized following the literature procedure.[18]

2.2. Radiochemistry

The radiolabeling of [^{11}C]MP-10 was accomplished by employing convenient conditions for methylation of *N*-desmethyl precursor with [^{11}C]MeI. Reaction of the desmethyl precursor **6** with [^{11}C]MeI was performed in DMF and in the presence of the NaH in DMF as outlined in Scheme 2 to give corresponding [^{11}C]MP-10 with approximately 45% yield and [^{11}C]**8** with approximately 36% yield after HPLC purification. The radiochemical purity of [^{11}C]MP-10 was greater than 92% and chemical purity was great than 95%. [^{11}C]MP-10 was identified by co-eluting with the solution of standard MP-10. The retention time of [^{11}C]MP-10 on the analytical HPLC system was 10.0–10.5 min. The entire synthetic procedure including the production of [^{11}C]MeI, HPLC purification and formulation of the radiotracer for vivo studies, was complete within 50–55 min. [^{11}C]MP-10 was obtained in a specific activity of ~370 GBq/μmol (decay corrected to EOB n = 15), which is sufficient for in vivo validation. However, while labeling [^{11}C]MP-10, we found that 1.5–4 equiv of NaH was necessary for the N-alkylation to obtain satisfactory yield. When aqueous NaOH solution was used, no product was obtained. In addition, adding the solution of NaH in DMF to the reaction vial 2–3 min prior to the [^{11}C] CH_3I delivery is necessary to obtain satisfactory yield. Either adding NaH in DMF too early or large excess of NaH in DMF will reduce radiolabeling yield. Solid phase extraction to process the HPLC collection fraction of the product prevents the final [^{11}C]MP-10 production from decomposition. When rotary evaporator was used to concentrate the [^{11}C]MP-10 product, the product [^{11}C]MP-10 decomposed easily.

2.3. Biodistribution

The radioactivity organ distribution after injection of [^{11}C]MP-10 into rats is summarized in Table 1. From 5 min to 60 min post-injection, [^{11}C]MP-10 displayed heterogenous distributions in the brain: the striatum displayed highest uptake compared to other brain regions. The percent injected doses per gram (%I.D./g) of the radioactivity post-injection of [^{11}C]MP-10 at 5, 30, and 60 min were 0.300 ± 0.094, 0.236 ± 0.035, and 0.164 ± 0.036 for striatum, 0.133 ± 0.025, 0.044 ± 0.009, and 0.044 ± 0.014 for cortex, 0.169 ± 0.049, 0.050 ± 0.010, and 0.051 ± 0.009 for hippocampus, 0.133 ± 0.023, 0.036 ± 0.003, and 0.035 ± 0.003 for cerebellum. These observations are consistent with the observation that striatum has the highest density of PDE10A whereas the density of PDE10A is relatively low in cortex.[2,16] The ratios of the striatum to non-target regions including blood, hippocampus, cortex and cerebellum reached 2.54, 1.88, 2.35, and 2.23 respectively, at 5 min; at 30 min, the ratios were 3.82, 4.80, 5.44, and 6.55 for striatum versus blood, hippocampus, cortex and cerebellum respectively. As shown in Figure 1, from 5 min to 30 min, the striatum: non-target ratios displayed an increase trend in rat brain, which suggested that radioactivity [^{11}C]MP-10 in the non PDE10A specific region was rapidly cleared. The higher striatum/organ ratios of [^{11}C]MP-10 and the increasing trend of striatum/organ ratios in rat brain indicated that [^{11}C]MP-10 has specific binding with PDE10A enriched-striatum. Among the peripheral tissues, the liver showed a relative high initial uptake of [^{11}C]MP-10, which reached 2.766 ± 0.350 (%I.D./g) in 5 min.; at 30 min the uptake of [^{11}C]MP-10 in liver still retained as 3.364 ± 0.613 (% I.D./g). There was a rapid clearance of the radioactivity from blood, lung, muscle, heart, kidney, and testes.

2.4. MicroPET studies

The results of the rodent brain distribution studies suggest that [^{11}C]MP-10 can be a suitable ligand for in vivo imaging of PDE10A. To confirm the feasibility of using [^{11}C]MP-10 to measure the levels of PDE10A in vivo, PET imaging studies of [^{11}C]MP-10 were conducted in three male rhesus monkeys (Fig. 2) on a microPET Focus 220 scanner. The representative summed images from 0 to 120 min were co-registered with MRI images to accurately identify the regions of interest. The summed images of MicroPET studies in male rhesus macaque post-injection of [^{11}C]MP-10 revealed high uptake of [^{11}C]MP-10 in caudate and putamen (Fig. 2 upper left) and give clear visualization of striatum, which is a region that expresses high level of the PDE10A. These data indicate: (a) [^{11}C]MP-10 can readily penetrate the blood–brain-barrier and enter into the non-human primate brain and, (b) the distribution of [^{11}C]MP-10 is consistent with the distribution of the PDE10A in brain. The tissue time–activity curves (Fig. 2 lower panel) indicate an increasing trend of radioactivity accumulation in caudate, putamen and cerebellum post-injection of [^{11}C]MP-10; Striatum: cerebellum ratio reaches maximum at 30 min post-injection of [^{11}C]MP-10 with

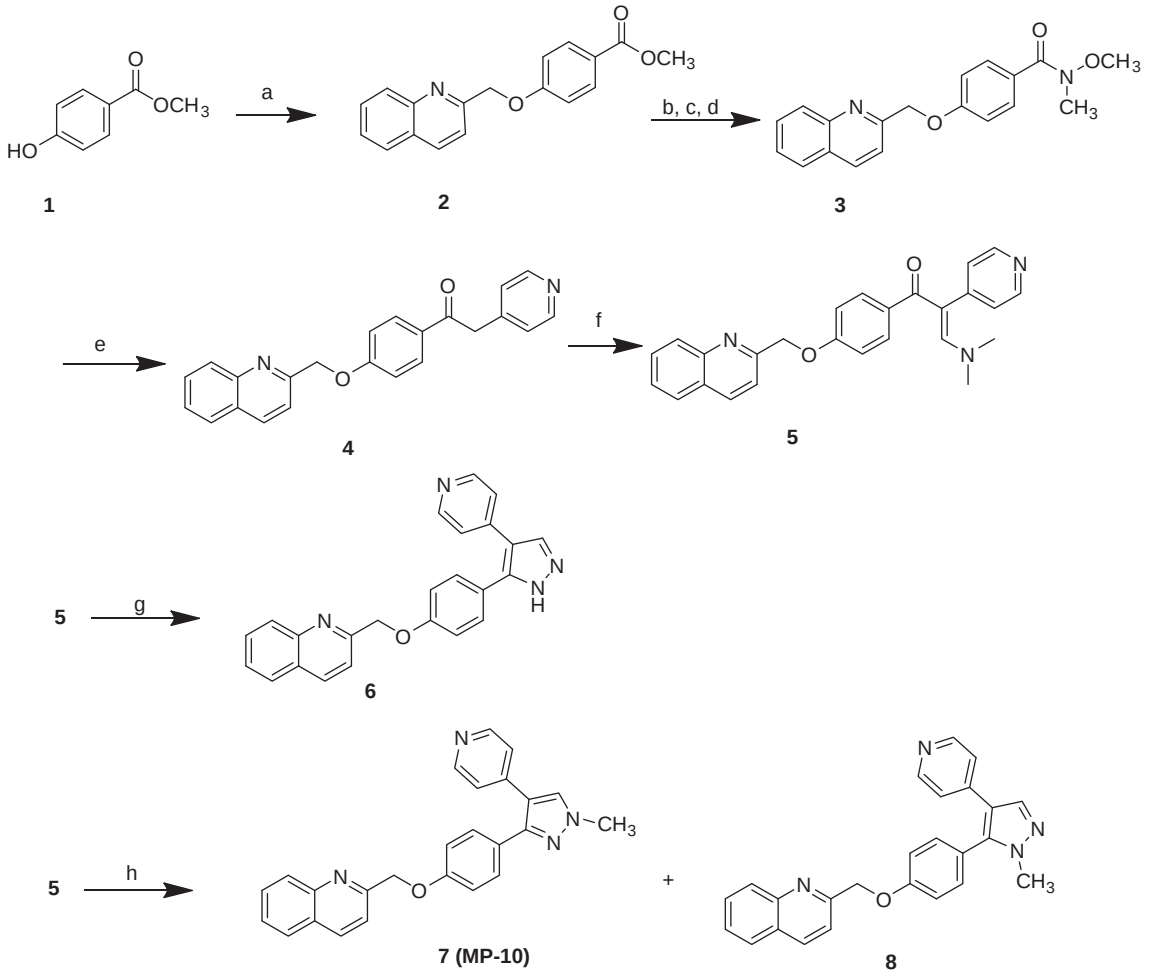

Reagent and Reaction condition:

(a) 2-(chloromethyl)quinoline, K_2CO_3/Acetone, Reflux; (b) NaOH, CH_3OH; (c) $SOCl_2$; (d) CH_3NHOCH_3/acetonitrile; (e) 4-methylpyridine, Lithium diisopropylamide (LDA); (f) 1,1-dimethoxy-*N*,*N*-dimethylmethanamine,reflux; (g) NH_2NH_2; (h) NH_2NHCH_3.

Scheme 1. Synthesis of MP-10.

a 2.0-fold ratio for caudate-to-cerebellum and 1.5-fold for putamen-to-cerebellum ratio. The increasing trend of radioactivity in the regions of interest may reflect a radiolabeled lipophilicity metabolite entering into the brain and accumulating in the brain regions.

2.5. Metabolite studies in monkey plasma, rat plasma as well as rat brain

2.5.1. In vivo metabolite analysis in rat blood and rat brain

To confirm whether or not radiolabeled metabolites enter the brain, the metabolite analysis of rat brain and rat plasma samples were performed post-injection of [^{11}C]MP-10 into Sprague–Dawley rats. The plasma radioactivity at 2 min post-injection displayed three radioactivity peaks. The percentage (%) of the three peaks is 1.23 for peak #1 (metabolite #1), a small amount (0.43) for peak #2 (metabolite #2) and a very large amount (98.35) for peak #3 which is the parent compound, [^{11}C]MP-10 (Table 2). At 20, 40, and 60 min post-injection of [^{11}C]MP-10, the percentages of the parent compound remained 74.20, 52.61, and 49.28; the percentages for metabolite #1 were 19.13, 35.19, and 40.72; the percentages for metabolite #2 are 5.06, 12.19, and 5.58. Overall, the parent compound [^{11}C]MP-10 in plasma decreased from 98.35 to 49.28. The percentage of metabolite #1 in plasma increased to 40.72 at 60 min (Fig. 3). The percentage of the metabolite #2 reached the highest of 12.19 at 40 min and then began to decrease.

For the rat brain samples, the percentages for [^{11}C]MP-10 were 98.71, 94.85, 84.74, and 78.62 at 2, 20, 40, and 60 min (Table 2). For metabolite #1, the percentages were 1.03, 3.45, 11.47, and 15.87 for 2, 20, 40, and 60 min brain tissue samples. The radioactive metabolite #1 was the major metabolite component that crossed the blood–brain-barrier and entered the brain. For metabolite #2, the percentages were 0.27, 0.93, 3.82, and 1.24 for 2, 20, 40, and 60 min brain tissue samples. Although metabolite #2 was found in the brain samples, it is negligible relative to metabolite #1 and to the parent compound. When comparing rat brain tissue HPLC data and rat plasma data at 60 min (Fig. 3), radioactive metabolite #1 was the major metabolite which had the capability of crossing the blood–brain-barrier and enter the brain. The accumulation of metabolite #1 in the brain resulted in increasing non-specific binding in the cerebellum.

To identify the structure of metabolite #1, the rats brain sample was co-injected into the LC–MS with cold compound 4-(1-methyl-4-(pyridin-4-yl)-1*H*-pyrazol-3-yl)phenol, the m/z^+ value of

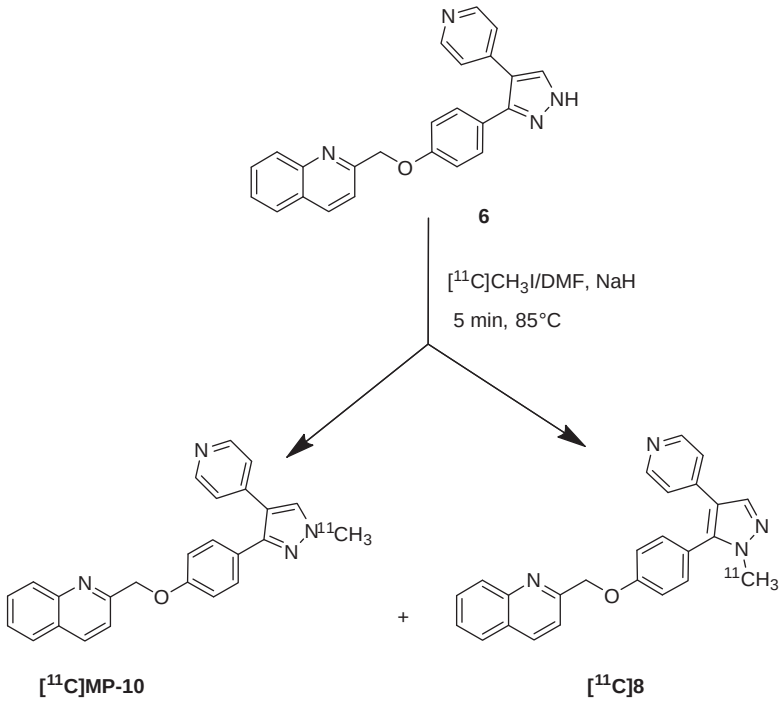

Scheme 2. Synthesis of [^{11}C]MP-10.

Table 1
Biodistribution of [^{11}C]MP-10 in male Sprague–Dawley rats (ID%/gram)

Organ	5 min	30 min	60 min
Blood	0.123 ± 0.033	0.065 ± 0.016	0.047 ± 0.012
Lung	0.317 ± 0.037	0.155 ± 0.053	0.090 ± 0.012
Liver	2.766 ± 0.350	3.395 ± 0.448	3.364 ± 0.613
Muscle	0.093 ± 0.021	0.059 ± 0.010	0.039 ± 0.011
Fat	0.124 ± 0.059	0.075 ± 0.020	0.100 ± 0.013
Heart	0.264 ± 0.080	0.102 ± 0.041	0.068 ± 0.023
Kidney	1.229 ± 0.215	0.366 ± 0.075	0.314 ± 0.060
Testes	0.160 ± 0.048	0.098 ± 0.006	0.068 ± 0.021
Total brain	0.162 ± 0.025	0.066 ± 0.008	0.056 ± 0.006
Brain regions			
Cortex[a,b]	0.133 ± 0.025	0.044 ± 0.009	0.044 ± 0.014
Hippocampus[a,b]	0.169 ± 0.049	0.050 ± 0.010	0.051 ± 0.009
Striatum	0.300 ± 0.094	0.236 ± 0.035	0.164 ± 0.036
Cerebellum[a,b]	0.133 ± 0.023	0.036 ± 0.003	0.035 ± 0.003

[a] *p*-Value <0.05 for striatum versus non-target tissue, 5 min.
[b] *p*-Value <0.005 for striatum versus non-target tissue, at 30 and 60 min.

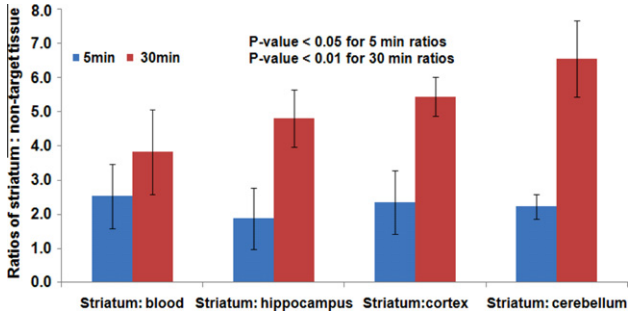

Figure 1. The striatum versus non-target tissue ratios of [^{11}C]MP-10 in were calculated by using the %ID/g data.

metabolite #1 was 251.2384, which matched with that of 4-(1-methyl-4-(pyridin-4-yl)-1*H*-pyrazol-3-yl)phenol (**9**), which suggested that radioactive 4-(1-[^{11}C]methyl-4-(pyridin-4-yl)-1*H*-pyrazol-3-yl)phenol was generated from the O-dealkylation [^{11}C]MP-10 post-injection, as outlined in Scheme 3.

2.5.2. The non-human primate plasma metabolite analysis

To check the metabolic stability of [^{11}C]MP-10 post-injection into non-human primates, radiolabeled metabolite analysis of monkey plasma sample was performed. HPLC analysis of rhesus macaque plasma samples at 5, 15, 30, and 60 min revealed only two radioactive peaks, a potential lipophilic metabolite (retention time ~3 min) and the parent compound; [^{11}C]MP-10 (retention time is ~10.5 min) were observed post-injection of [^{11}C]MP-10 as shown in Figure 4. The first radioactive peak in the HPLC chromatogram of rhesus plasma has the same retention time as the radioactive metabolite #1 from rat brain tissue and rat plasma samples. However, in rhesus monkey plasma, only one radiolabeled peak, metabolite #1 were observed in the HPLC chromatograms. This observation is consistent with the metabolite analysis result from the fluorine version of MP-10 analogue, ^{18}F-JNJ41510417.[22] The metabolite #2 in the rat plasma sample as a minor lipophilic metabolite was not observed in the arterial blood samples of rhesus monkeys. The difference in metabolism results from rat and monkey plasma may reflect species differences. Similar results also were observed in previous studies.[24–26] Nonetheless, metabolism of the radiotracer in rat is still a valuable predicator for metabolism in non-human primate, which will be used as a selection criteria to determine if a PET tracer has potential to serve as a PDE10A PET probes for further evaluations in non-human primate and human being.

3. Materials and methods

3.1. General

All analytical grade chemicals and reagents were purchased from Sigma–Aldrich (Milwaukee, WI) and were used without further purification unless otherwise specified. Flash column

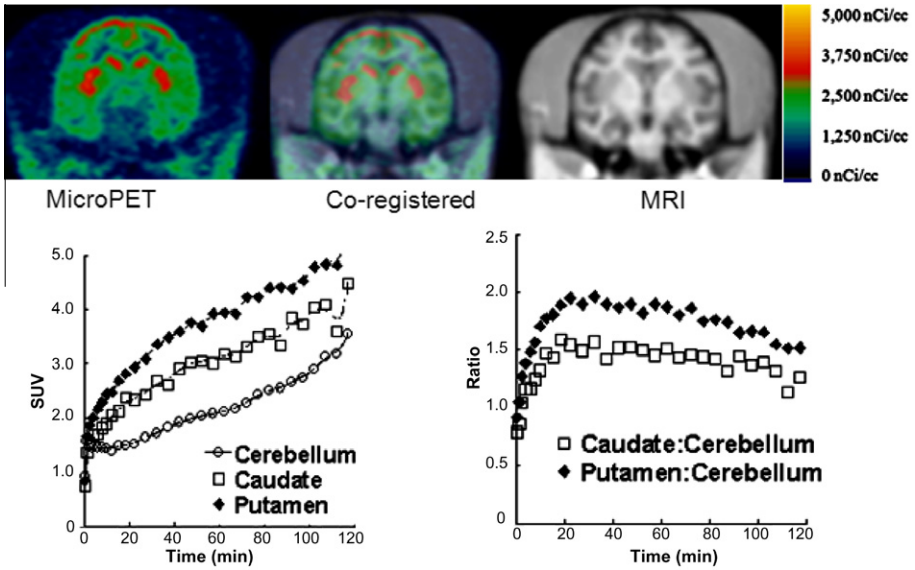

Figure 2. Upper panel: MicroPET images (left), co-registered images (middle) and MRI images (right), High uptake of [^{11}C]MP-10 in striatum was observed which gave clear visualization of tracer in putamen and caudate; lower panel: tissue time–activity curves for caudate, putamen and cerebellum (left); target: non-target ratios (right).

Table 2
Metabolite analysis of [^{11}C]MP-10 in rat brain and plasma

Time (min)	Brain tissue			Plasma		
	% Peak #1	% Peak #2	% [^{11}C]MP-10	% Peak #1	% Peak #2	% [^{11}C]MP-10
2	1.03	0.27	98.71	1.23	0.43	98.35
20	3.45	0.93	94.85	19.13	5.06	74.20
40	11.47	3.82	84.74	35.19	12.19	52.61
60	15.87	1.24	78.62	40.72	5.58	49.28

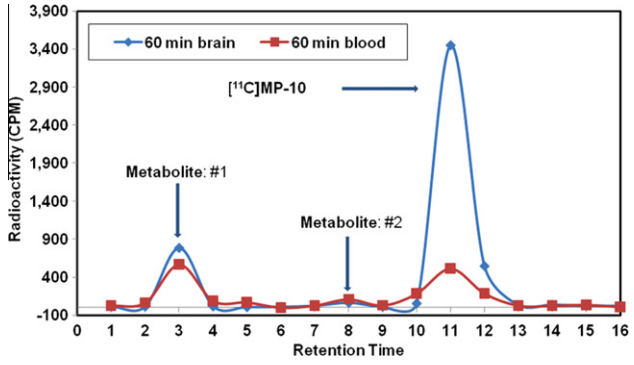

Figure 3. HPLC results of rat plasma and brain tissue at 60 min post-iv injection of [^{11}C]MP-10 into rats. Metabolite #1 that is the major metabolite in both plasma and brain tissue has the capability of crossing the brain–blood-barrier and enter into the brain.

chromatography was conducted using Scientific Adsorbents, Inc. silica gel, 60 Å, '40 Micron Flash' (32–63 μ). Melting points were determined using MEL-TEMP 3.0 apparatus and uncorrected. ^{1}H NMR spectra were recorded at 300 MHz on a Varian Mercury-VX spectrometer with $CDCl_3$ or DMSO-d_6 as solvent and tetramethylsilane (TMS) as the internal standard. All chemical shift values are reported in ppm (δ). Peak multiplicities were recorded as singlet, S; double, d; triplet, t, multiplet, m. Elemental analyses (C, H) were determined by Atlantic Microlab, Inc. (Norcross, GA).

3.2. Chemistry

The synthesis of MP-10 precursor (**6**) and reference compound (**7**) was accomplished by following procedure reported in the literature with slight modifications.[18] The synthetic approach is outlined in Scheme 1. The experimental details for the synthesis of the intermediates (**2**–**5**, **9**), precursor (**6**), the reference compound (**7**) and its isomer **8** were provided in Supplementary data.

3.3. Radiochemistry

3.3.1. Production of [^{11}C] CH_3I

Briefly, [^{11}C]CH_3I was produced from [^{11}C]CO_2 using a GE PETtrace MeI Microlab.[27] Up to 51.8 GBq of [^{11}C]CO_2 was produced from Washington University's JSW BC-16/8 cyclotron by irradiating a gas target of 0.2% O_2 in N_2 for 15–30 min with a 40 μA beam of 16 MeV protons. The GE PETtrace MeI microlab coverts the [^{11}C]CO_2 to [^{11}C]CH_4 using a nickel catalyst (Shimalite-Ni,[28] Shimadzu, Japan P.N.221-27719) in the presence of hydrogen gas at 360 °C; it was further converted to [^{11}C]CH_3I by reaction with iodine that was held in a column in the gas phase at 690 °C. Approximately 12 min after EOB, several hundred millicuries of [^{11}C]CH_3I were delivered as a gas to the hot cell where the radiosynthesis was accomplished.

3.3.2. Radiosynthesis of [^{11}C]MP-10

A stream of [^{11}C]CH_3I in helium was bubbled for 5 min into a solution of **6** (1.5–2.0 mg) in DMF (0.18 mL) and 30 μL of sodium hydride in DMF solution (3 mg of NaH (95%) in 250 μL DMF) at 0 °C (ice-water bath). The sealed reaction vessel was heated at 85 °C (oil bath)

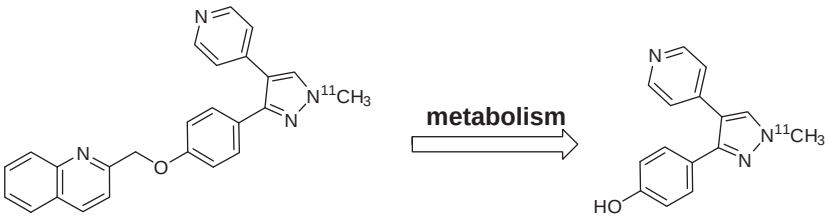

[^{11}C]MP-10
Log P*[a] = 3.52

Radiolabed metabolite #1 (9)
Log P = 1.4

*[a]: Calculated using the program ACD/log D when the pH = 7.4.

Scheme 3. *O*-Dealkylation of [^{11}C]MP-10.

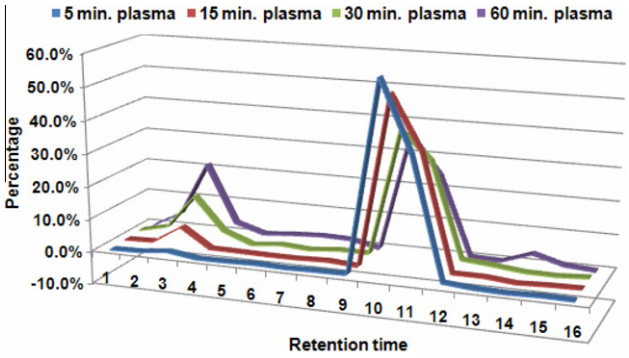

Figure 4. HPLC results of monkey arterial blood plasma at 5, 15, 30, and 60 min post-iv injection of [^{11}C]MP-10 into monkeys. Only one metabolite with a retention time of 3 min was observed and it matched the metabolite #1 in the rat plasma and brain tissue post-iv injection of [^{11}C]MP-10. This metabolite has the capability of crossing the brain–blood-barrier and entering into the brain.

for 5 min. The reaction was quenched by adding HPLC solvent (1.8 mL), and the diluted solution was injected to a high-performance liquid chromatography (HPLC) Agilent Zorbax SB-C18 reverse phase column (9.4 × 250 mm); the product was eluted by using acetonitrile/0.1 M ammonium formate buffer (40:60, v/v) at pH ~4.5 as the mobile phase, at a flow rate of 4.0 mL/min and the UV detection was at 254 nM. Under these conditions, the retention time of the precursor **6** was ~12.1 min; the retention time of the [^{11}C]MP-10 was ~19.90 min; the retention time of the other isomer [^{11}C]**8** was ~22.53 min. The [^{11}C]MP-10 product was collected into a vial containing 50 mL milli-Q water and passed through a Sep-Pak Plus C-18 cartridge (Waters, Milford, MA, USA), in which the product was trapped. The trapped product was eluted with ethanol (0.6 mL) followed by 5.4 mL of 0.9% saline. After sterile filtration into a dose vial, the final product was ready for quality control (QC) analysis and animal studies. The HPLC was performed on Agilent SB C-18 reverse phase analytic HPLC column (250 mm × 4.6 mm, 5 μA) and UV detection at 254 nm wavelength. The mobile phase was acetonitrile/0.1 M ammonium formate buffer (45:55, v/v) using 1.2 mL/min flow rate. Under these conditions the retention time of [^{11}C]MP-10 was 10.4 min. The radioactive dose sample was authenticated by co-injection with the cold reference compound MP-10. The radiochemical purity was >92%, the chemical purity was >95%, the labeling yield was ~45% (n = 15, decay corrected to EOB) and the specific activity was >370 GBq/μmol (decay corrected to EOB).

3.4. Biodistribution studies

All animal experiments were conducted in compliance with the Guidelines for the Care and Use of Research Animals established by Washington University's Animal Studies Committee. For the biodistribution studies, 3.7×10^{-3}–5.55×10^{-3} GBq of [^{11}C]MP-10 in 100–150 μL of saline containing 10% ethanol was injected via the tail vein into mature male Sprague–Dawley rats (425–490 g) under 2–3% isoflurane/oxygen anesthesia. Groups of at least four rats were used for each time point. At 5 min, 30 min and 60 min pi, the groups of rats were again anesthetized and euthanized. The whole brain was quickly removed and dissected into segments consisting of striatum, hippocampus, cortex, and cerebellum. The remainder of the brain was also collected to determine total brain uptake. At the same time, samples of blood, lung, liver, muscle, fat, heart, brain and testes were removed and counted in a Beckman Gamma 8000 well counter with a standard dilution of the injectate. Tissues were weighed, and the %ID/g was calculated. The striatum/organ ratios were calculated by dividing the %ID/g of the striatum by the %ID/g of the non-target tissue.

3.5. Imaging studies in male rhesus monkeys

MicroPET studies of [^{11}C]MP-10 were performed on three adult male rhesus monkeys (~7–12 kg) with a microPET Focus 220 scanner. The animals were fasted for 12 h before PET study. The animals were initially anesthetized using intramuscular ketamine (10–20 mg/kg) and glycopyrollate (0.13–17 mg/kg) and then transported to the PET scanner suit. Upon arrival, the animal was intubated with an endotracheal tube and anesthesia was maintained at 0.75–2.0% isoflurane/oxygen throughout the PET scanning procedure. After intubation, a percutaneous venous catheter was placed for radiotracer injection. The temperature was kept constant at 37 °C with a heated water blanket. In each microPET scanning session, the head was positioned supine in the adjustable head holder with the brain in the center of the field of view. A 10 min transmission scan was performed to check the position; once confirmed, a 45 min transmission scan was obtained for attenuation correction. Subsequently, a 2 h dynamic emission scan was acquired after administration of 0.22–0.37 GBq of [^{11}C]MP-10 via the venous catheter.

3.5.1. MicroPET image processing and analysis

Acquired list mode data were histogrammed into a 3D set of sinograms and binned to the following time frames: 3 × 1 min, 4 × 2 min, 3 × 3 min, and 20 × 5 min. Sinogram data were corrected for attenuation and scatter. Maximum a posteriori (MAP) reconstructions were done with 18 iterations and a β value of 0.004. A 1.5 mm Gaussian filter was applied to smooth each MAP reconstructed image. These images were then co-registered with MRI images to accurately identify the regions of interest with Amira software (Visage Imaging, Inc., Carlsbad, CA). The 3D regions of interest were manually drawn through all planes of co-registered MRI images for the caudate, putamen, and cerebellum

(Fig. 2 upper left). The regions of interest then were overlaid on all reconstructed PET images to obtain time–activity curves. Activity measurements were standardized to body weight and dose of radioactivity injected to yield standardized uptake value (SUV) (Fig. 2 lower left).

3.6. Metabolite studies in monkey plasma, rat plasma as well as rat brain

3.6.1. In vivo metabolite analysis in rat blood and rat brain

Adult male Sprague–Dawley rats (250–300 g) were anesthetized with 2–3% isoflurane/oxygen and [^{11}C]MP-10 (~0.04 GBq for the 2 min, ~0.19 GBq for the 20 min, ~0.24 GBq for 40 min; ~0.28 GBq for 60 min) was administered via intravenous tail vein injection. Whole blood samples were collected via cardiac puncture under anesthesia into heparinized syringes immediately before rats were euthanized. Rats were euthanized under anesthesia at 2, 20, 40, and 60 min post-injection. The whole brain was removed from the rat, blotted to remove excess blood, and homogenized on ice with 2 mL of ice-cold acetonitrile. 1 mL aliquots of whole blood were counted in a well counter and then separated by centrifugation for 2 min into packed red cells (PRC) and plasma, which were separated and counted. An aliquot of serum was deproteinated by mixing with 2 parts of ice-cold acetonitrile; plasma proteins were separated by centrifugation, and both portions were counted. 200 μL of the supernatant was injected on an Agilent SB C-18 analytic HPLC column (250 mm × 4.6 mm, 5 μA) and peaks detected at 254 nm UV wavelength. The mobile phase was acetonitrile/0.1 M ammonium formate buffer (48:52, v/v) and the flow rate was 1.0 mL/min. The HPLC fractions were collected at 1 min intervals for 16 min; the sample radioactivity was counted and decay corrected to the time the first sample of the series was counted. Similarly, a 1 mL aliquot of the brain homogenate was transferred to a separate tube and counted in a well counter. The acetonitrile extract was separated from the tissue pellet by centrifugation. The supernatant was used for HPLC chromatography as described above. The percent of unchanged [^{11}C]MP-10 (parent compound) and radiolabeled metabolites was calculated by dividing the amount of recovered radioactivity in the peak by the sum of the total recovered radioactivity in all samples and multiplying by 100. The parent compound [^{11}C]MP-10 was authenticated by co-injection with cold standard MP-10 sample; the retention time for [^{11}C]MP-10 was ~10.5 min. It was observed that even using the same brand of analytic column for the metabolite analysis, in order to keep the similar retention time of [^{11}C]MP-10 as ~10 min, the mobile phase and the flow rate needs to be adjusted. To further determine the structure of metabolite #1 which is the first radioactivity peak in the HPLC chromatograph, 60 min of brain tissue supernatant sample (180 μL) was co-injected with 4-(1-methyl-4-(pyridin-4-yl)-1*H*-pyrazol-3-yl)phenol acetonitrile solution (10 μL, 100 ppm) into a LC–MS, in which the liquid chromatography condition was the same as HPLC condition described above. From the LC–MS analysis, the metabolite peak #1 was detected to have m/z^+ as 251.2384, which matched with 4-(1-methyl-4-(pyridin-4-yl)-1*H*-pyrazol-3-yl)phenol.

3.6.2. In vivo metabolite analysis in macaque plasma

Arterial blood samples (1.2–1.5 mL) were collected at 5, 15, 30, and 60 min post-iv injection of [^{11}C]MP-10. The HPLC injection sample preparation and data collection were conducted by following the similar procedure as described for rat plasma samples.

4. Conclusion

In summary, [^{11}C]MP-10, a high affinity and high selectivity ligand for enzyme PDE10A was successfully radiosynthesized by methylating the corresponding desmethyl precursor with [^{11}C]CH_3I in DMF in the presence of sodium hydride as the base. Biodistribution study of [^{11}C]MP-10 was conducted in male Sprague–Dawley rats and found that the highest uptake in the brain was in the striatum, the PDE10A enriched region. The highest target to non-target (striatum to cerebellum) ratio was found to be 6.55 at 30 min post-injection. The microPET studies performed in rhesus monkeys revealed that [^{11}C]MP-10 readily enters the brain of non-human primates and its accumulation was more specific to PDE10A enriched-striatum. However, tissue time–activity curve displayed an increase in the radioactivity accumulation in striatum and cerebellum, post-injection of [^{11}C]MP-10. Analysis of the metabolites from rat brain tissue, plasma and monkey plasma post-injection of [^{11}C]MP-10 revealed that a lipophilic radiolabeled metabolite was formed. This metabolite has the capability to penetrate blood–brain-barrier and enter into the brain. Overall, [^{11}C]MP-10 was found to bind specifically to PDE10A in the rat and monkey brain and displayed a clear image of striatum, to identify a clinical PET probe to image PDE10A in human beings. Further optimization of the structure of [^{11}C]MP-10 is necessary to resolve the issue of radioactive metabolite.

Acknowledgment

Financial support for these studies was provided by the National Institute of Health under 5R33MH081281-04 (RHM), NS058714, 1R21NS061025-01A2 and Intramural grant MIR-11-009 of Mallinckrodt Institute of Radiology in Washington University School of Medicine. The authors gratefully thank Christina M. Zukas, John Hood, Darryl Craig, Ruike Wang, Aixiao Li and Junfeng Li for their excellent technical assistance for the microPET studies in non-human primate.

Supplementary data

Supplementary data associated with this article can be found, in the online version, at doi:10.1016/j.bmc.2011.01.032.

References and notes

1. Loughney, K.; Snyder, P. B.; Uher, L.; Rosman, G. J.; Ferguson, K.; Florio, V. A. *Gene* **1999**, *234*, 109.
2. Bora, R. S.; Gupta, D.; Malik, R.; Chachra, S.; Sharma, P.; Saini, K. S. *Biotechnol. Appl. Biochem.* **2008**, *49*, 129.
3. Hebb, A. L.; Robertson, H. A. *Curr. Opin. Pharmacol.* **2007**, *7*, 86.
4. Nishi, A.; Kuroiwa, M.; Miller, D. B.; O'Callaghan, J. P.; Bateup, H. S.; Shuto, T.; Sotogaku, N.; Fukuda, T.; Heintz, N.; Greengard, P.; Snyder, G. L. *J. Neurosci.* **2008**, *28*, 10460.
5. Coskran, T. M.; Morton, D.; Menniti, F. S.; Adamowicz, W. O.; Kleiman, R. J.; Ryan, A. M.; Strick, C. A.; Schmidt, C. J.; Stephenson, D. T. *J. Histochem. Cytochem.* **2006**, *54*, 1205.
6. Groenewegen, H. J.; van den Heuvel, O. A.; Cath, D. C.; Voorn, P.; Veltman, D. J. *Brain Dev.* **2003**, *25*, S3.
7. Winterer, G.; Carver, F. W.; Musso, F.; Mattay, V.; Weinberger, D. R.; Coppola, R. *Hum. Brain Mapp.* **2007**, *28*, 805.
8. Winterer, G.; Weinberger, D. R. *Trends Neurosci.* **2004**, *27*, 683.
9. DeLong, M. R.; Wichmann, T. *Arch. Neurol.* **2007**, *64*, 20.
10. Menniti, F. S.; Chappie, T. A.; Humphrey, J. M.; Schmidt, C. J. *Curr. Opin. Investig. Drugs* **2007**, *8*, 54.
11. Hebb, A. L; Robertson, H. A; Denovan-Wright, E. M. *Neuroscience* **2004**, *123*, 967.
12. Hu, H.; McCaw, E. A.; Hebb, A. L.; Gomez, G. T.; Denovan-Wright, E. M. *Eur. J. Neurosci.* **2004**, *20*, 3351.
13. Siuciak, J. A.; Chapin, D. S.; Harms, J. F.; Lebel, L. A.; McCarthy, S. A.; Chambers, L.; Shrikhande, A.; Wong, S.; Menniti, F. S.; Schmidt, C. J. *Neuropharmacology* **2006**, *51*, 386.
14. Schmidt, C. J.; Chapin, D. S.; Cianfrogna, J.; Corman, M. L.; Hajos, M.; Harms, J. F.; Hoffman, W. E.; Lebel, L. A.; McCarthy, S. A.; Nelson, F. R.; Proulx-LaFrance, C.; Majchrzak, M. J.; Ramirez, A. D.; Schmidt, K.; Seymour, P. A.; Siuciak, J. A.; Tingley 3rd, F. D.; Williams, R. D.; Verhoest, P. R.; Menniti, F. S. *J. Pharmacol. Exp. Ther.* **2008**, *325*, 681.
15. Threlfell, S.; Sammut, S.; Menniti, F. S.; Schmidt, C. J.; West, A. R. *J. Pharmacol. Exp. Ther.* **2009**, *328*, 785.
16. Chappie, T.; Humphrey, J.; Menniti, F.; Schmidt, C. *Curr. Opin. Drug Discov. Dev.* **2009**, *12*, 458.

17. Walker, M. A. *Drug Discovery Today* **2010**, *15*, 79.
18. Verhoest, P. R.; Chapin, D. S.; Corman, M.; Fonseca, K.; Harms, J. F.; Hou, X.; Marr, E. S.; Menniti, F. S.; Nelson, F.; O'Connor, R.; Pandit, J.; Proulx-LaFrance, C.; Schmidt, A. W.; Schmidt, C. J.; Suiciak, J. A.; Liras, S. *J. Med. Chem.* **2009**, *52*, 5188.
19. Kehler, J.; Kilburn, J. P. *Expert Opin. Ther. Pat.* **2009**, *19*, 1715.
20. Tu, Z.; Xu, J.; Jones, L. A.; Li, S.; Mach, R. H. *Nucl. Med. Biol.* **2010**, *37*, 509.
21. Tu, Z.; Xu, J.; Li, S.; Jones, L. A.; Mach, R. H. *J. Nucl. Med.* **2009**, *50*, 618.
22. Celen, S.; Koole, M.; De Angelis, M.; Sannen, I.; Chitneni, S. K.; Alcazar, J.; Dedeurwaerdere, S.; Moechars, D.; Schmidt, M.; Verbruggen, A.; Langlois, X.; Van Laere, K.; Andres, J. I.; Bormans, G. *J. Nucl. Med.* **2010**, *51*, 1584.
23. Moerlein, S. M.; Perlmutter, J. S.; Cutler, P. D.; Welch, M. *J. Nucl. Med. Biol.* **1997**, *24*, 311.
24. Honer, M.; Hengerer, B.; Blagoev, M.; Hintermann, S.; Waldmeier, P.; Schubiger, P. A.; Ametamey, S. M. *Nucl. Med. Biol.* **2006**, *33*, 607.
25. Osman, S.; Lundkvist, C.; Pike, V. W.; Halldin, C.; McCarron, J. A.; Swahn, C. G.; Ginovart, N.; Luthra, S. K.; Bench, C. J.; Grasby, P. M.; Wikstrom, H.; Barf, T.; Cliffe, I. A.; Fletcher, A.; Farde, L. *Nucl. Med. Biol.* **1996**, *23*, 627.
26. Pike, V. W.; McCarron, J. A.; Hume, S. P.; Ashworth, S.; Opacka-Juffry, J.; Osman, S.; Lammertsma, A. A.; Poole, K. G.; Fletcher, A.; White, A. C.; Cliffe, I. A. *Med. Chem. Res.* **1994**, *5*, 208.
27. Tu, Z.; Chu, W.; Zhang, J.; Dence, C. S.; Welch, M. J.; Mach, R. H. *Nucl. Med. Biol.* **2005**, *32*, 437.
28. Andrews, T. C.; Brooks, D. J. *Mol. Med. Today* **1998**, *4*, 532.